OPEN

Highly directional bottom-up 3D nanoantenna for visible light

L. Tong[1]*, T. Pakizeh[2], L. Feuz[1] & A. Dmitriev[1]

[1]Department of Applied Physics, Chalmers University of Technology, Göteborg 41296, Sweden, [2]Faculty of Electrical and Computer Engineering, K. N. Toosi University of Technology, Tehran 16314, Iran.

Correspondence and requests for materials should be addressed to T.P. (T.Pakizeh@eetd. kntu.ac.ir) or A.D. (alexd@chalmers.se)

* Current address: Institute of Physics, Chinese Academy of Sciences, Beijing 100190, P. R. China.

Controlling light at the nanoscale is of fundamental importance and is essential for applications ranging from optical sensing and metrology to information processing, communications, and quantum optics. Considerable efforts are currently directed towards optical nanoantennas that directionally convert light into strongly localized energy and vice versa. Here we present highly directional 3D nanoantenna operating with visible light. We demonstrate a simple bottom-up approach to produce macroscopic arrays of such nanoantennas and present a way to address their functionality via interaction with quantum dots (QDs), properly embedded in the structure of the nanoantenna. The ease and accessibility of this structurally robust optical antenna device prompts its use as an affordable test bed for concepts in nano-optics and nanophotonics applications.

The manipulation of light at the nanoscale requires controlled delivery of the optical radiation to the tightly focused sub-wavelength spot, where conventional optics is fundamentally limited by the diffraction of light[1,2]. To achieve this, considerable efforts are directed towards optical nanoantennas. The notion of an optical nanoantenna has emerged over the past decade as means of translating the manipulation principles of radio-frequency electromagnetic (EM) radiation to the nanoscale, achieving impressive light control over nanoscale EM landscapes[3,4]. All-dielectric antennas featured compact dimensions and high directionality have been recently shown at the single nanoparticles' level[5,6]. More importantly, nanoantennas that use localized surface plasmon resonances (LSPRs) provide new ways to collect, manipulate and deliver light in nanophotonics[7–9], photovoltaics[10], and optoelectronics[11]. Interestingly, the concepts of radio-frequency antenna design turned out to be applicable to the optical frequency regime. A prominent example of the latter is the adoption of the classical Yagi-Uda antenna to function in the near-IR[12–19]. An important issue with such direct adoption is the different response of metals in the optical frequency regime (Drude-like)[20] that can be, in principle, circumvented by the proper scaling of the nanoantenna material properties[21,22]. Other limitations include nanoantenna dimensions that frequently surpass the operating wavelength, the intrinsic need of a substrate and/or surrounding polymer matrix on which functional optical elements are fabricated and utilized, and, stemming from the above, the need of non-trivial experimental strategies to actually couple or decouple near-field signals to or from such nanodevices.

Here we bring forward a 3D nanoantenna that operates in the *visible regime* with high directivity. Different from the 3D plasmonic nanoarchitectures for THz domain[23–25], here we have all functional elements available to efficiently couple, in practice, the local optical emitters. These nanoantennas are easily produced in a macroscopic array format using affordable bottom-up nanofabrication – hole-mask colloidal lithography (HCL).

Results

There are three basic elements of this nanoantenna, which we designate as 'I', 'II' and 'III',followed by their sequential increase in size (Fig. 1A). Each element is a metal nanodisk, supporting a LSPR, which is separated from the neighboring elements by a dielectric spacer. Directional emission or reception is realized into free-space, which is faced by the smallest element (I) of the device. The dimensions of the dielectric spacers are in-line with the size of the functional elements, making this nanoantenna-type rather compact. Such design can be experimentally realized by HCL – a bottom-up nanofabrication based on colloidal self-assembly (see Experimental Section)[26,27]. Short-range ordered arrays of nanoantennas typically span over cm[2] and can be produced on a large variety of substrates – here we choose regular microscope glass slides, with antenna elements made of Au, spaced by silica (c.f. scanning electron microscopy (SEM) image on Fig. 1B, featuring both the overall shape of the nanodevices (left) and resolved plasmonic elements (right)). The design structure is verified by optical reflectance
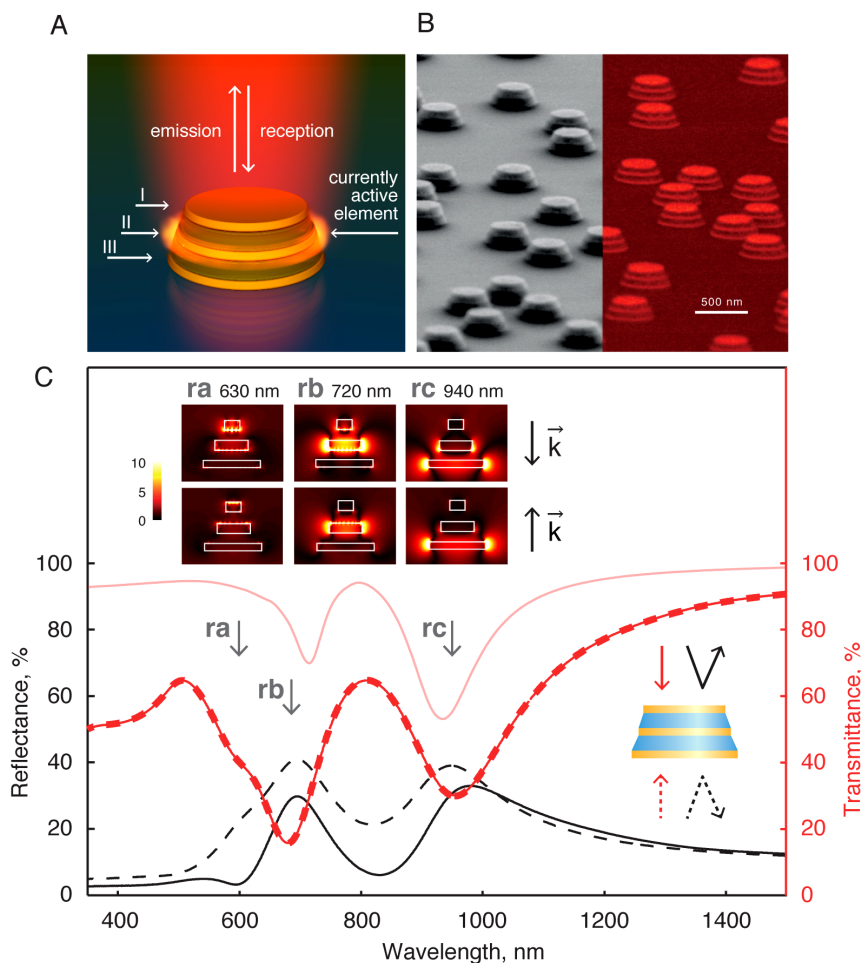
Figure 1 | (A) Schematics of the nanoantenna elements marked 'I', 'II' and 'III' and spaced by dielectrics, and directionality function – i.e., far-field-to-near-field conversion: emission or reception modes are available via proper coupling to or from either of the elements (in this example – element II), (B) SEM of the nanoantennas on a glass substrate revealing their overall shape (left) and their elements (right, backscattered electrons image); (C) Far-field and near-field optical design: experimental reflectance (black) and transmittance (red) (solid – forward, dashed – backward, right inset – schematics of illumination) and simulated near-field plots at the corresponding far-field spectral features with backward and forward illumination (left inset). Three resonant features are marked 'ra', 'rb' and 'rc'.

and transmittance and by simulating the near-fields with finite-difference time-domain (FDTD) numerical calculations (Fig. 1C)[27,28]. Whereas transmittance through the nanoantenna array is directionless due to reciprocity (red solid and dashed curves in Fig. 1C) and displays three basic spectroscopic features (marked 'ra', 'rb' and 'rc' in Fig. 1C), the reflectance shows remarkable asymmetry with respect to the direction of incidence (compare black solid and dotted curves in Fig. 1C). This asymmetry is most pronounced in the visible and near-IR. While electrodynamics simulations overall match the far-field optical spectra (light red curve in Fig. 1C, calculated for the structure with the elements of 200 nm, 120 nm and 50 nm and corresponding thickness of 20 nm, spacer 50 nm), the detailed nature of the spectral features can be identified with simulated near-field plots (inset of Fig. 1C). In the FDTD simulations, the effective refractive index for the surrounding medium is n = 1.25, which partially addresses the substrate influences on the LSPRs of the nanodisks and their optical interactions in the proposed nanoantenna. However, the slight discrepancies between the measurements and calculations (see Fig. 2C) might be assigned to the substrate effects. From these we mark that back illumination allows addressing sequentially elements II and III as we move along the spectra towards longer wavelengths (lower row of Fig. 1C inset, note that the element I is hardly ever excited this way). Front illumination largely features elements, addressed simultaneously in pairs (I–II and II–III as

followed the top row of the Fig. 1C inset from 630 nm to 940 nm plot). Note also that while the best near-field signal is normally produced at the lateral sides of the elements, a sizable EM field enhancement exists between the elements and on top of the nanoantenna in the visible.

The present nanoantenna measures roughly one third of the operating wavelength in all three dimensions. Such compact configuration allows the three elements to be electromagnetically coupled in all regimes, namely at the near-, intermediate-, and far-field. This distinguishes the present case from so far reported multi-element optical nanoantennas, particularly inspired by the low-frequency Yagi-Uda concept, where functional elements are spatially separated, individually addressed and provide an antenna' directionality function due to the far-field coupling[12,15]. The EM interactions in the near- and intermediate-field regimes are predominant because of the compact configuration in the present case. These strong optical interactions trigger new hybridized plasmonic resonances in the structure, similar to those observed in strongly coupled nanoplasmonic geometries[29–31].

To address the performance of this nanoantenna in the directional near- to far-field conversion, we turn to the quantum dots (QDs) that have been previously used to feed nanoantennas elements[15]. As mentioned earlier, the highest EM field enhancement is produced at the sides of the nanoantenna elements due to the largely dipolar
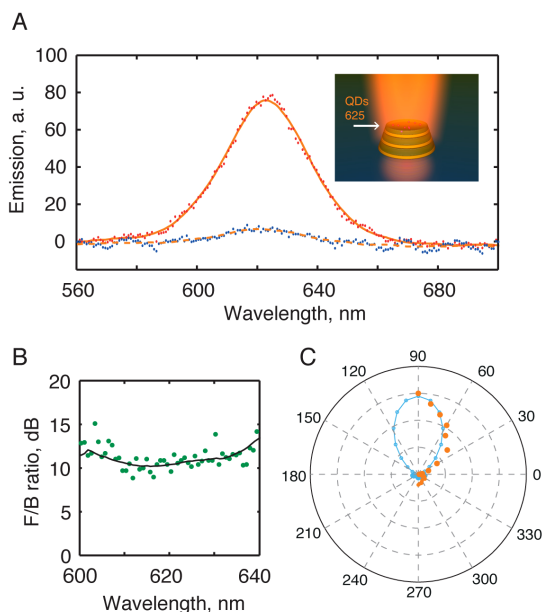
Figure 2 | (A) The directionality function of the nanoantenna is probed by the CdSe QDs with excitation at 532 nm and emission at 625 nm, coupled to the element I: forward – red dots and solid fit, backward – blue dots and dashed fit, inset – schematics of QDs positioning. The emission spectra are accompanied by (B) experimentally obtained directionality, dotted green and solid black – from experimental points and fitted data, respectively, extracted from (A); and (C) emission' polar plots, with dotted orange as experimental emission (see SI for details), and dotted blue – as modeled with FDTD.

character of the involved plasmonic resonances. We choose, however, to embed QDs into the dielectric spacers *between* the elements to preserve the robustness of the design with the outlook for possible applications in integrated nanophotonics. We introduce CdSe QDs (excitation – at 532 nm, emission – at 625 nm) on top of element I, embedded in a silica layer (schematics inset in Fig. 2A). Exciting QDs with a laser (for the schematics of the experimental setup – see Fig. S1), we further detect free-space propagating light (Fig. 2A) at the characteristic emission line of the employed QDs, peaking at around 625 nm that overlaps with the 'ra' resonance of element I. Note that this resonance is detected as a shoulder-like feature in transmittance (Fig. 1C). Such emission is characterized by a forward-to-backward (F/B) directionality that effectively surpasses 10 dB (Fig. 2B). The directionality stays rather constant in the entire emission range (Fig. 2B), which suggests that it is the light produced by the QDs emission that is further processed by the nanoantenna and is beamed as a directional free-space EM radiation. The directional emission pattern is further corroborated by the emitted intensity' polar plots, both experimental and calculated with FDTD (Fig. 2C). It is instrumental to follow the emergence of such strong directionality by constructing one- or two-element nanoantennas, and combining them with the QDs at different wavelengths. The QDs that emit light at 625 nm and 780 nm were similarly used to 'feed' one-element (Figs. S2 A, C, D) and two-element (Figs. S2 B, E, F) configurations. Whereas one-element conventional dipolar plasmonic nanodisk antennas show largely bidirectional light emission (see insets in Figs. S2 C, D, note also the stronger emission enhancement for the case of 780 nm QDs, which are better spectrally tuned to the resonance of the sole nanoantenna element – Fig. S2 A), two-element nanoantennas already feature a promising F/B-directionality on the order of 3 dB (see insets in Figs. S2 E, F). Due to the strongly near-field-coupled response of the nanoantenna elements, properly matching local emitters spectrally to a selected one of the

three resonances promotes the strong directionality of the emitted radiation. The local EM field enhancement pattern should be taken into account for the best coupling to a selected resonance. By using the quantum emitter at 780 nm, that is – matching the 'rb' resonance of the nanoantenna – the far-field propagating light receives similar directionality. This can be followed in Fig. 3. Fig. 3A shows the far-field spectral response of the antenna sample immersed in refractive index matching oil. This makes 'ra', 'rb' and 'rc' resonances to red-shift to 660 nm, 787 nm and 1055 nm, respectively (compare to Fig. 1C). With 'rb' resonance positioned now close to the QDs emission peak, the F/B ratio of emission remains $\sim$ 10 dB around the peak, as shown in Fig. 3B. Additionally, we mark here a sizable decrease in the emission intensity (compare to Fig. 2A, for example).

The enhancement of the QDs emission and its connection to the directionality for this class of nanoantennas can be followed in Fig. 4. Keeping the wavelength of the QDs fixed (625 nm, Figs. 4A, C and 780 nm, Figs. 4B, D), we experimentally raster the positioning of these 'feeding elements' through the nanoantenna stack. The best near-field coupling and directionality for the 625 nm QDs is achieved when they are positioned above element I (compare Fig. 2A with Figs. 4A and 4C, insets – wavelength-dependent directionality plots). For 780 nm QDs, the best directionality is realized when they are similarly positioned above the element I (Fig. 3B), but the best light emission enhancement is attained when the emitters are above element II instead (Fig. 4B). Note that the latter scenario provides poorer emission directionality on the order of 3–5 dB (inset of Fig. 4B). The plasmonic resonant modes here can be easily manipulated by varying the number of elements, inter-element spacing, their aspect ratios and the surrounding refractive index medium. Additionally, the positioning of the feeding sources and thus the choice of the feeding strategy are flexible due to the possibility to directly address any of the nanoantenna elements.

Discussion
Though fabricated on a supporting substrate, this plasmonic nanoantenna can in principle be lifted from the substrate[32,33], and, as the QDs are tightly embedded in the structure, we envision that the directional emission will be preserved. This also suggests that due to its 3D-articulated structure, the role of the substrate is inferior for the nanoantenna integrity and function – similarly to semi-shells[32] standard transfer with, for example, a polydimethylsiloxane (PDMS) stamp, would provide a substrate-free array of these nanodevices. Of further practical interest, denser HCL-produced arrays of nanodisks display an exciting interplay between far-field coupling and near-field 'hot-spot' patterns[12]. It is reasonable to foresee that in the present array increasing the density might result in unexpected effects on directionality and functionality of the whole platform. Another facet of the potential functionality of these devices is highlighted in the context of the currently rising research theme of nanoantenna-enhanced processes[23,34]. Excitingly, the outlined nanoantennas class can be readily adopted for such development[35]. Overall, this practical model nanoantenna system paves the way for the development and engineering of novel nanophotonic devices aiming at tailoring the optical radiation at a nanoscale. And with the ease of serial bottom-up nanofabrication, such potential devices can be straightforwardly tested and adopted.

Methods
Nanoantenna fabrication. The nanoantennas were fabricated using the HCL method[26], a versatile and cost-efficient method that facilitates the fabrication of short-range-ordered arrays of nanostructures on various surfaces. Briefly, PMMA (Microchem Coorporation, 4 wt% diluted in anisole, MW = 950000) was spin-coated on cleaned glass and baked at 110°C for 10 min to form a $\sim$ 200 nm thick film. Oxygen plasma (50 W, 5 s, 250 mTorr, Plasma Therm Batchtop RIE 95 m) was then applied to produce a hydrophilic surface. An aqueous solution of poly(diallyldimethylammonium chloride) (PDDA, 0.2 wt%, MW 200000–350000, Sigma Aldrich) and a suspension of sulfate polystyrene (PS) nanobeads (0.2 wt%, nominal diameter $\sim$ 150 nm, Invitrogen) were sequentially drop casted on the
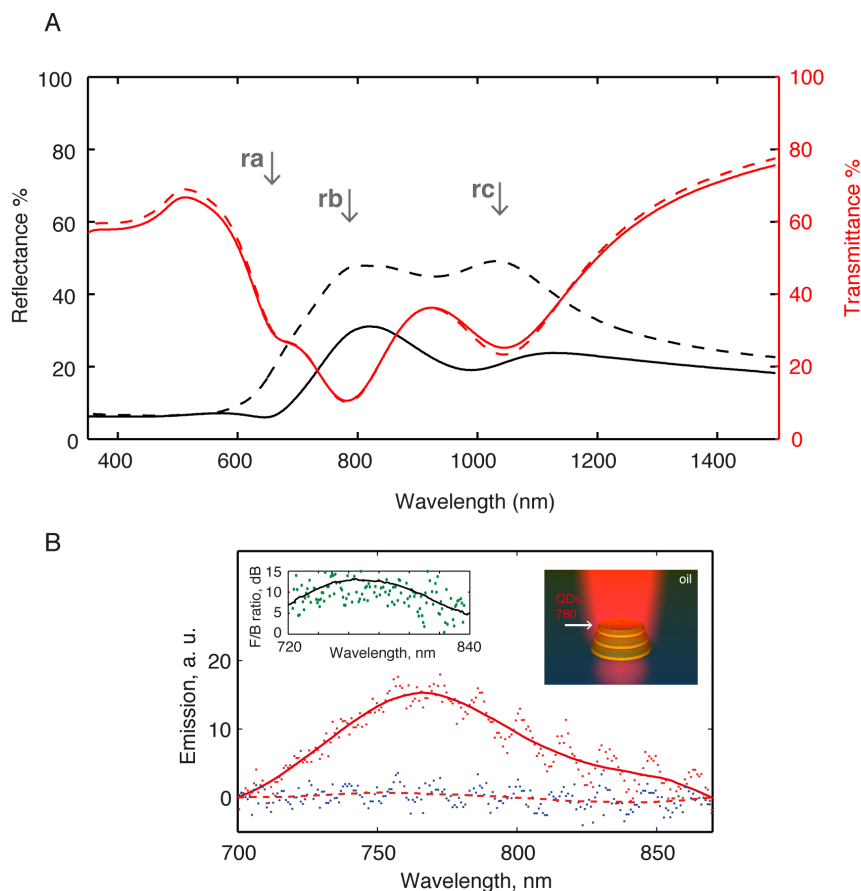
Figure 3 | Tuning the 'rb' resonance to the QDs emitting at 780 nm. The 'rb' resonance shifts to ∼ 780 nm by immersing the nanoantennas in refractive index matching oil (RI = 1.55). (A) Forward (solid) and backward (dashed) reflectance (in black) and transmittance (in red) of three-disk nanodevice in oil. (B) QD 780 nm emissions and F/B curve, showing a directionality that slightly surpasses 10 dB (dots – experimental data, solid and dashed lines – fits from fitted spectral data). Inset: schematics of the three-disk nanodevice.
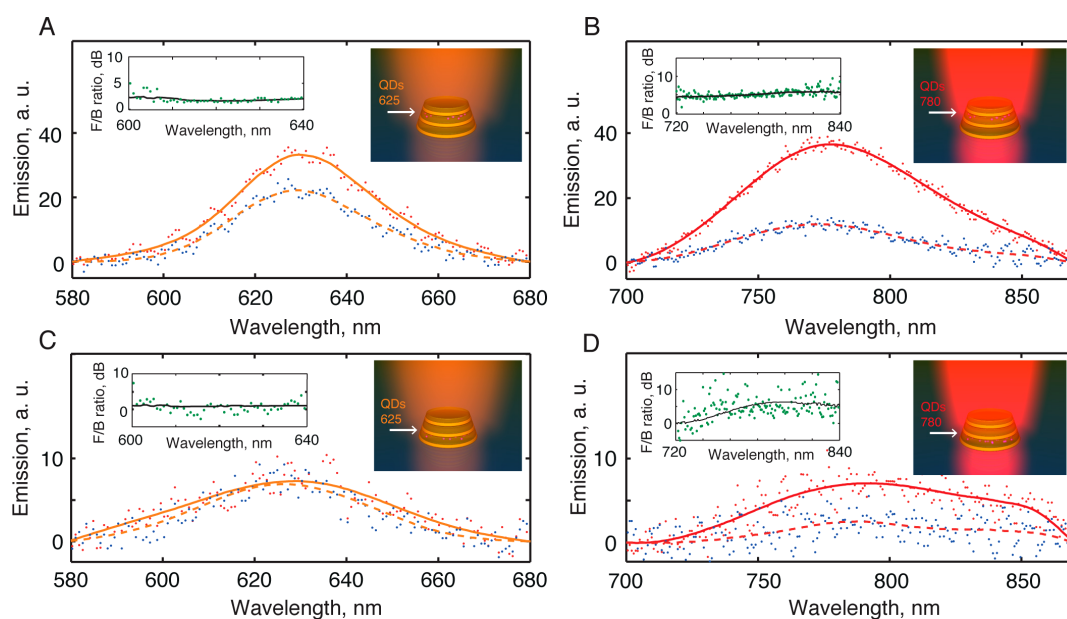

Figure 4 | QDs emission modification. QDs emitting at 625 nm and at 780 nm are positioned on top of element II (A, B) or on top of element III (C, D). Dotted – experimental emission data (red – forward, blue – backward), solid lines – fitted forward, dashed – fitted backward. Insets – corresponding spectrally resolved forward-to-backward emission ratios in dB, dotted – from experimental data points, solid – from the fitted data.

sample for 30 s, each rinsed by ultrapure water and dried by purified N_2. A short-range ordered array of PS nanobeads on the PMMA film was thus obtained. A thin gold film (10 nm) was thermally evaporated on the sample as a sacrificial mask, followed by tape-striping to remove the PS nanobeads. PMMA underneath the nanoholes in the gold film was adequately removed using O_2 plasma etching. Desired materials were then deposited and arrays of nanodisks were obtained after liftoff in acetone. The sequence of materials deposition for the ultracompact nanobeamers was determined as follows: 20 nm gold, 50 nm SiO_2, 28 nm gold, 50 nm SiO_2 and 30 nm gold. Between each two layers, 1 nm Ti was deposited to improve adhesion. Note that the size and thickness of the gold disks can be freely changed to tune the resonance of the elements to match the QDs emission.

QDs embedding. Streptavidin conjugated CdSe quantum dots were purchased from Invitrogen. A 5 nm SiO_2 thin film was deposited on the desired gold disk as a dielectric spacer to avoid fluorescence quenching of the QDs. The sample was then taken out from the evaporator chamber and etched by O_2 plasma at 50 W for 10 s to produce hydrophilicity. A droplet of diluted QDs solution ($\sim 3 \times 10^{-8}$ M, which arithmetically assures a monolayer of QDs on the whole area of a sample of $\sim 1.5 \times 2.0$ cm^2) was drop casted on the sample, dried in air, and immediately gently rinsed by ultrapure water and dried by N_2. The sample was then transferred back to the evaporator chamber for deposition of the other materials. If the QDs are on the top gold disk, a 15 nm SiO_2 film was deposited to embed the QDs.

T and R measurements. Transmission and reflection measurements were carried out on a Cary 5000 UV-vis-NIR spectrophotometer (Agilent). A specular reflection accessory was used for reflection measurements.

QDs emission measurements. QDs emission spectra at different angles were measured using a home-made setup (see experimental schematic in Fig S1). Samples were excited by a 532 nm laser (Millennia Pro, Spectra-Physics) slightly focused (half-cone angle $\sim 6°$) on the front side with the nanobeamers. The incident angle was fixed at 45 degrees. A fiber-coupled spectrometer (Ocean Optics QE5000) mounted on a rotation stage was used to measure the emission spectra at different angles ($-90° \sim 90°$). A notch filter (NF532) was used in front of the collection fiber to remove the elastic scattering of the laser.

Directionality plot calculations with FDTD. The nanobeamer is properly excited by a single oscillating electric Hertzian-dipole that is situated on top of the smallest element, according to the experimental realization. The radiation pattern of the dipole is strongly modified due to the excitations and interactions of the LSPRs in the nearfield[28]. The radiation pattern of the dipole is calculated based on the Huygens' principle, connecting the calculated near-field to the far-field. That is, at any operating wavelength and polar angle, the radiated optical intensity is calculated.

1. Frey, H. G., Witt, S., Felderer, K. & Guckenberger, R. High-resolution imaging of single fluorescent molecules with the optical near-field of a metal tip. *Phys. Rev. Lett.* **93**, 200801 (2004).
2. Kinkhabwala, A. *et al.* Large single-molecule fluorescence enhancements produced by a bowtie nanoantenna. *Nature Photon.* **3**, 654–657 (2009).
3. Novotny, L. & van Hulst, N. Antennas for light. *Nature Photon.* **5**, 83–90 (2011).
4. Biagioni, P., Huang, J. S. & Hecht, B. Nanoantennas for visible and infrared radiation. *Rep. Prog. Phys.* **75**, 024402 (2012).
5. Person, S. *et al.* Demonstration of zero optical backscattering from single nanoparticles. *Nano Lett.* **13**, 1806–1809 (2013).
6. Fu, Y. H., Kuznetsov, A. I., Miroshnichenko, A. E., Yu, Y. F. & Luk'yanchuk, B. Directional visible light scattering by silicon nanoparticles. *Nat. Commun.* **4**, 1527 (2013).
7. Esteban, R., Teperik, T. V. & Greffet, J. J. Optical patch antennas for single photon emission using surface plasmon resonances. *Phys. Rev. Lett.* **104**, 026802 (2010).
8. Gramotnev, D. K. & Bozhevolnyi, S. I. Plasmonics beyond the diffraction limit. *Nature Photon.* **4**, 83–91 (2010).
9. Schuller, J. A. *et al.* Plasmonics for extreme light concentration and manipulation. *Nature Mater.* **9**, 193–204 (2010).
10. Spinelli, P. *et al.* Optical impedance matching using coupled plasmonic nanoparticle arrays. *Nano Lett.* **11**, 1760–1765 (2011).
11. Knight, M. W., Sobhani, H., Nordlander, P. & Halas, N. J. Photodetection with active optical antennas. *Science* **332**, 702–704 (2011).
12. Dorfmuller, J. *et al.* Near-field dynamics of optical Yagi-Uda nanoantennas. *Nano Lett.* **11**, 2819–2824 (2011).
13. Coenen, T., Vesseur, E. J. R., Polman, A. & Koenderink, A. F. Directional emission from plasmonic Yagi-Uda antennas probed by angle-resolved cathodoluminescence spectroscopy. *Nano Lett.* **11**, 3779–3784 (2011).
14. Kosako, T., Kadoya, Y. & Hofmann, H. F. Directional control of light by a nano-optical Yagi-Uda antenna. *Nature Photon.* **4**, 312–315 (2010).
15. Curto, A. G. *et al.* Unidirectional emission of a quantum dot coupled to a nanoantenna. *Science* **329**, 930–933 (2010).
16. Dregely, D. *et al.* 3d optical Yagi-Uda nanoantenna array. *Nat. Commun.* **2**, 267 (2011).
17. Staude, I. *et al.* Broadband scattering by tapered nanoantennas. *Phys. Status Solidi - RRL* **6**, 466–468 (2012).
18. Maksymov, I. S., Staude, I., Miroshnichenko, A. E. & Kivshar, Y. S. Optical Yagi-Uda nanoantennas. *Nanophotonics* **1**, 65–81 (2012).
19. Miroshnichenko, A. E. *et al.* An arrayed nanoantenna for broadband light emission and detection. *Phys. Status Solidi - RRL* **5**, 347–349 (2011).
20. Balanis, C. A. *Antenna theory: Analysis and design.* 3rd edn, (Wiley, 2005).
21. Novotny, L. Effective wavelength scaling for optical antennas. *Phys. Rev. Lett.* **98**, 266802 (2007).
22. Bryant, G. W., De Abajo, F. J. G. & Aizpurua, J. Mapping the plasmon resonances of metallic nanoparticles. *Nano Lett.* **8**, 631–636 (2008).
23. Liu, N., Hentschel, M., Weiss, T., Alivisatos, A. P. & Giessen, H. Three-dimensional plasmon rulers. *Science* **332**, 1407–1410 (2011).
24. Liu, N., Liu, H., Zhu, S. N. & Giessen, H. Stereometamaterials. *Nature Photon.* **3**, 157–162 (2009).
25. Liu, N. *et al.* Three-dimensional photonic metamaterials at optical frequencies. *Nature Mater.* **7**, 31–37 (2008).
26. Fredriksson, H. *et al.* Hole-mask colloidal lithography. *Adv. Mater.* **19**, 4297–4302 (2007).
27. Dmitriev, A. *et al.* Enhanced nanoplasmonic optical sensors with reduced substrate effect. *Nano Lett.* **8**, 3893–3898 (2008).
28. Pakizeh, T. & Käll, M. Unidirectional ultracompact optical nanoantennas. *Nano Lett.* **9**, 2343–2349 (2009).
29. Agio, M. Optical antennas as nanoscale resonators. *Nanoscale* **4**, 692–706 (2012).
30. Prodan, E., Radloff, C., Halas, N. J. & Nordlander, P. A hybridization model for the plasmon response of complex nanostructures. *Science* **302**, 419–422 (2003).
31. Yu, N. F. *et al.* Light propagation with phase discontinuities: Generalized laws of reflection and refraction. *Science* **334**, 333–337 (2011).
32. Zhang, Y., Barhoumi, A., Lassiter, J. B. & Halas, N. J. Orientation-preserving transfer and directional light scattering from individual light-bending nanoparticles. *Nano Lett.* **11**, 1838–1844 (2011).
33. Dmitriev, A., Pakizeh, T., Käll, M. & Sutherland, D. S. Gold-silica-gold nanosandwiches: Tunable bimodal plasmonic resonators. *Small* **3**, 294–299 (2007).
34. Schumacher, T. *et al.* Nanoantenna-enhanced ultrafast nonlinear spectroscopy of a single gold nanoparticle. *Nat. Commun.* **2**, 333 (2011).
35. Shegai, T. & Langhammer, C. Hydride formation in single palladium and magnesium nanoparticles studied by nanoplasmonic dark-field scattering spectroscopy. *Adv. Mater.* **23**, 4409–4414 (2011).

Acknowledgments

Author contributions

T.P., A.D. and L.T. conceived the idea. A.D. and L.T. designed the experiment, T.P. performed electrodynamics simulations, L.T. fabricated nanoantennas and performed the experiments, L.F. developed QDs placement strategy, all authors participated in discussion of the results and took part in writing the manuscript.

Additional information

Supplementary information accompanies this paper at http://www.nature.com/scientificreports

Competing financial interests: The authors declare no competing financial interests.

How to cite this article: Tong, L., Pakizeh, T., Feuz, L. & Dmitriev, A. Highly directional bottom-up 3D nanoantenna for visible light. *Sci. Rep.* **3**, 2311; DOI:10.1038/srep02311 (2013).